Colloids and Surfaces A: Physicochem. Eng. Aspects 441 (2014) 776–785

Contents lists available at ScienceDirect

Colloids and Surfaces A: Physicochemical and Engineering Aspects

journal homepage: www.elsevier.com/locate/colsurfa

Evaporation of a sessile water drop on a heated surface with controlled wettability

Elizaveta Ya. Gatapova[a,b,*], Andrey A. Semenov[a], Dmitry V. Zaitsev[a], Oleg A. Kabov[a,c]

[a] Kutateladze Institute of Thermophysics, Siberian Branch of Russian Academy of Sciences, 1 Lavrentyev Avenue, 630090 Novosibirsk, Russia
[b] Novosibirsk State University, 2 Pirogova Street, 630090 Novosibirsk, Russia
[c] National Research Tomsk Polytechnic University, 30 Lenin Avenue, 634050 Tomsk, Russia

HIGHLIGHTS

- The temperature difference is 40 °C.
- The heat exchange with atmosphere is found to contribute to the temperature field.
- Increase of the evaporative mass flux near the contact line.
- At the final stage of the drop life the specific evaporation rate abruptly increases.
- The specific evaporation rate is inversely proportional to the contact radius.

GRAPHICAL ABSTRACT

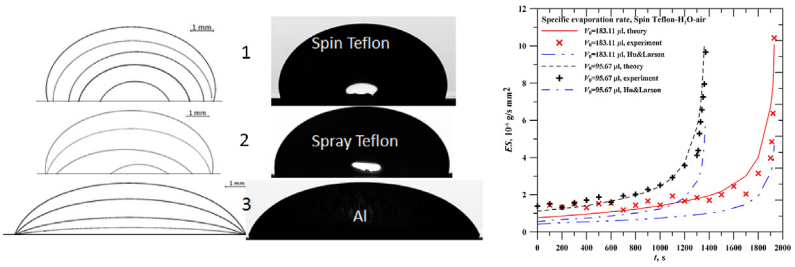

ARTICLE INFO

Article history:
Received 16 April 2013
Received in revised form 9 May 2013
Accepted 10 May 2013
Available online 28 May 2013

Keywords:
Contact angle hysteresis
Evaporation
Liquid drop
Heated substrate
Temperature difference
Heat transfer

ABSTRACT

This paper presents an experimental and theoretical study of the evaporation of a sessile water drop to open atmosphere when the temperature difference between the solid substrate and the atmosphere is about 40 °C. Using substrates with different wettability we investigate all three modes of droplet evaporation: pinning, partial pinning and depinning. One of the most important results is that at the final stage of the drop life the specific evaporation rate abruptly increases especially for drops with small and moderate contact angle hysteresis. The coupled heat and mass transfer model is considered where the temperature field on the drop surface determines the distribution of vapor concentration on liquid–gas interface. The heat exchange of liquid drop with gas phase strongly affects the temperature distribution on the droplet surface. There is an appreciable increase of temperature close to periphery of the droplet near the contact line. And this leads to increasing of evaporative mass flux near the contact line. We calculate the evaporation rate and conclude that the global evaporation rate is proportional to the contact radius r_b while the drop area is proportional to the drop contact radius squared r_b^2. Thus, the specific evaporation rate (evaporation rate per drop area) is a function of $1/r_b$ and diverges at the end of the evaporation when the drop contact radius tends to zero. The calculated specific evaporation rate is in excellent agreement with the experimental data.

* Corresponding author at: Kutateladze Institute of Thermophysics, Siberian Branch of Russian Academy of Sciences, 1 Lavrentyev Avenue, 630090 Novosibirsk, Russia. Tel.: +7 9134646679; fax: +7 3833308480.
E-mail address: gatapova@itp.nsc.ru (E.Ya. Gatapova).

0927-7757/$ – see front matter © 2013 Elsevier B.V. All rights reserved.
http://dx.doi.org/10.1016/j.colsurfa.2013.05.046

1. Introduction

The problem of the evaporation of a liquid drop has been known for many years [1,2] and recently again attracted the interest of many researchers. This problem is particularly actual in microfluidics, where evaporation plays crucial role for the small droplet size. A drop deposited on a solid substrate forms together with solid and gas phases the triple contact line. Understanding of evaporation and heat transfer processes in a liquid drop and near the contact line is very important for many industrial applications such as microelectronics, micro- and nano-fabrication, ink jet printing, and other fields.

A lot of theoretical and experimental studies of the evaporating droplet with small capillary size exist in the literature. The diffusive evaporation rates depend on contact angle [3] and the investigations of the substrate nature effect [4] still remain an important issue. The evaporation of sessile drops of pure liquids is satisfactorily described by model of Hu and Larson [5] based on a purely diffusive evaporation mass flux for the case of natural evaporation at ambient temperature. The recent achievements on the topic are presented by review of Erbil [6]. However, the coupled heat and mass transfer problem when the substrate is heated still requires more analysis and understanding. Such studies are important for understanding of the heat transfer enhancement as well as contact line dynamics.

We would like to briefly review a few papers that are directly relevant to thermal effects of the solid substrate on evaporation of a sessile liquid droplet to open atmosphere. An experimental and theoretical investigations of the effect of atmosphere on the evaporation of the pinned sessile water droplet were performed by Sefiane et al. [7]. They studied the influence of three different ambient gases at reduced pressure. Reducing the atmospheric pressure leaded to increasing the evaporation rate due to increasing the diffusion coefficient of water vapor in atmosphere. Coupled heat conduction equations for two solid–liquid phases and the diffusion equation in gas phase were considered. Heat transfer equation in the gas phase was neglected. The vapor concentration on the liquid–gas interface was increasing function on temperature and it was approximated as a fourth-degree polynomial function of the temperature.

The effect of the substrate thermal conductivity and substrate thickness on the evaporation of a sessile water drop was investigated numerically in [8] using a quasi-steady state diffusion model for a non-heated solid substrate. Both pinned and depinned cases were considered. The heat conduction equations for all three solid–liquid–gas phases as well as diffusion equation in gas phase with appropriate boundary condition were considered. The dependence of vapor concentration on liquid–gas interface on temperature was the same as in [7]. The temperature of the bottom side of the solid substrate and the temperature of the atmosphere far away from the droplet were considered to be equal. The temperature difference between the drop base and drop surface is obtained to be less than 1.1 K for different solid thermal conductivity. A cooling of the drop to 16 °C was found for ambient temperature 25 °C. There exists an important effect of the thermal resistance of the substrate when decreasing its thermal conductivity or increasing its thickness. This was discussed also in [9].

For the relatively large temperature difference between the heated substrate and the ambient gas $T_w - T_g$, the convective thermal transport in gas phase becomes of great importance and should be carefully investigated. The empirical model accounting the combined diffusive and convective transport has been developed by authors of [10,11]. The convective contribution to the evaporation rate was estimated by a correlation with Grashof number.

In this paper we present the experimental results on investigations of evaporating water droplet on a heated substrate with different wettability properties as well as the theoretical analysis of the influence of the temperature difference $T_w - T_g$ on heat transfer and on evaporation of a sessile water drop.

2. The problem description

2.1. Physical formulation

We analyze experimentally and theoretically the evaporation of the heated sessile drop of relatively large size to open atmosphere (Fig. 1). Drop of pure liquid is deposited on a heated solid substrate with controlled wettability. The drop is heated and the quasi-steady heat transfer state is reached between the liquid drop and the solid surface. A pure distilled deionized nanofiltered water is used as the working liquid having a large latent heat of vaporization. The temperature difference between the solid substrate and the atmosphere $T_w - T_g$ is about 40 °C. The use of water allows us to analyze the temperature difference impact on evaporation intensity and heat transport. The initial volume of the drop is relatively large (80–400 μl), so that the gravity can affect the drop profile. The wetted area is a circle with a radius r_b. We investigate three modes of droplet evaporation: (1) at constant contact angle – without pinning of contact line, (2) at constant contact area – full pinning of contact line and (3) a complex of two previous modes – partial pinning of contact line.

2.2. Experimental setup and apparatus

A scheme of the test section and imaging system used in our experiments is presented in Fig. 2. Two optical techniques are used for experimental measurements: shadow method and infrared technique. The shadow method consists of a LED coupled with a lens creating a parallel beam of light and a NIKON D300S camera with a macro lens (Nikon 105 mm f/2.8 G IF-ED AF-S VR) used to record the shadow profile of the drop. The spatial resolution of the system is 6 micron/pixel, and the speed varies from 3 to 8 fps. Shadow images are processed by the Drop Shape Analysis software (KRUSS), which allows determination of the drop profile (by the Young–Laplace equation) and also all geometrical parameters of the liquid drop such as the base diameter, maximum diameter, height, volume, the contact angles (right, left, mean), the surface area, the area of the base.

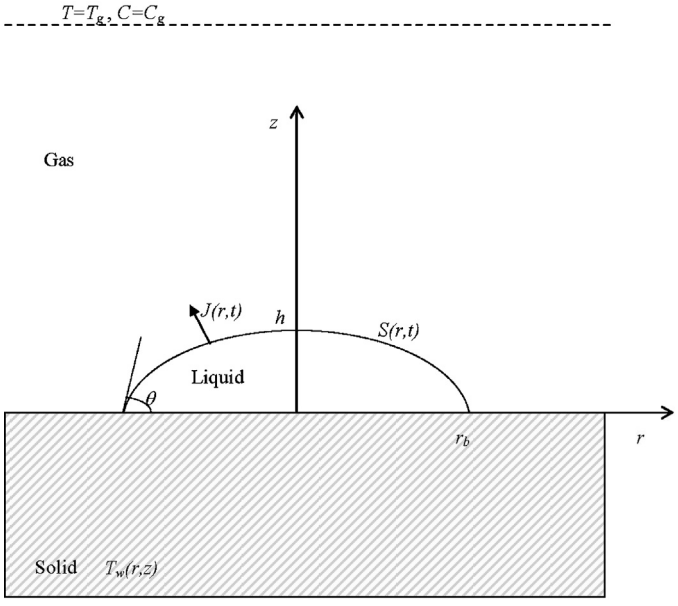

Fig. 1. Scheme of a sessile liquid drop.

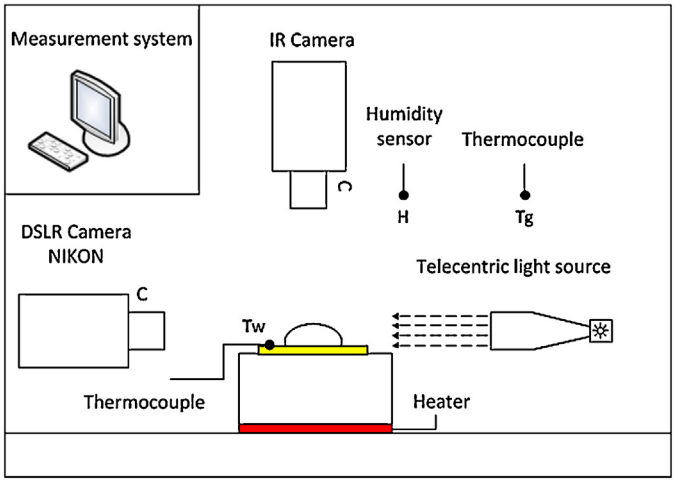

Fig. 2. Experimental setup.

IR-scanner is placed perpendicular to the test surface and records a liquid drop from the top. In this work we use the infrared scanner for visualization purposes only – to control the drop axial symmetry. The emissivity of the substrate is much smaller than the emissivity of water, so the drop boundary is clearly visible in IR. We use Xenics GOBI-2075 infrared scanner with a maximum frequency of 25 Hz at full resolution 384 × 288 pixels. Pixel size is 25 μm × 25 μm, spectral range of the matrix is in the range of 8–15 μm. We successfully used this technique previously to study the dry patch formation and evolution in heated liquid films [12].

As test substrates we use glass discs of thickness 3.2 mm and diameter 2 in. coated with coverings with different wettability: Spin Teflon-coated by spinning molten droplets of Teflon (contact angle hysteresis is defined as the difference between the advancing and receding contact angles, $\theta_h = \theta_a - \theta_r = 122.5^\circ - 112.7^\circ = 9.8^\circ$), Spray Teflon-coated by spraying molten droplets of Teflon ($\theta_h = 119.9^\circ - 90.6^\circ = 29.3^\circ$), HMDS-covering performed by hot vapor deposition on a cold substrate of hexamethyldisilazane ($\theta_h = 95.3^\circ - 69.3^\circ = 26.0^\circ$). In addition, one of the substrates is made of anodized aluminum uncoated ($\theta_h = 84.8^\circ - 13.4^\circ = 71.4^\circ$). A Peltier element is used as a heater placed on the bottom side of aluminum plate with thickness of 50 mm (Fig. 2). A test substrate is placed on the aluminum plate. The substrate temperature was measured with the help of a thermocouple located on the test surface at the distance of 10–15 mm from the drop boundary. The temperature at this point was kept constant (64 °C) during the evaporation process. In the following sections, first, we analyze theoretically the possible influence of the heat transport to ambient gas phase and evaporation intensity on droplet cooling. Next, we present an experimental data on contact radius and contact angles evolutions during droplet evaporation on different substrates. And finally, we investigate experimentally and theoretically the local mass flux and the specific evaporation rate.

3. Heat and mass transfer to gas phase analysis

In this section we analyze the heat transfer from the "hot" droplet surface to gas phase and discuss the possible influence of the convection to ambient gas and evaporation intensity on droplet cooling in quasi-stationary situation.

A cylindrical coordinate system is used with radial coordinate r and axial coordinate z (Fig. 1). For small drop with a contact radius r_b less than the capillary length $l = \sqrt{\sigma/\rho_l g}$ (equal to 2.6 mm for water at a temperature of 64 °C) a spherical cap shape is commonly used. For relatively large drop it does not work and we apply the ellipsoidal cap geometry [13] in order to include the possible influence of the gravity. The function $S(r, t)$ defines the surface of the droplet as:

$$S(r,t) = b\sqrt{1 - \frac{r^2}{a^2}} - \frac{h^2}{r_b \tan\theta - 2h} \quad (1)$$

for $r \le r_b$, where h is a height of the drop, $a = r_b\left(r_b\tan\theta - h\right)/\sqrt{r_b\tan\theta\left(r_b\tan\theta - 2h\right)}$ and $b = h\left(r_b\tan\theta - h\right)/(r_b\tan\theta - 2h)$ are semi-major and semi-minor axes. Note that the inverse problem for determination of the contact angle can be solved:

$$\tan\theta = \frac{2\left(1-e^2\right)r_b h}{\left(1-e^2\right)r_b^2 - h^2} \quad (2)$$

where $e = \sqrt{1-(b^2/a^2)}$ is the eccentricity of ellipse. Fig. 3 illustrates an evolution of a pinned water drop on anodized aluminum with contact radius $r_b = 4.95$ mm and demonstrates an excellent agreement of the ellipsoidal drop shape with experimental data obtained using the Young–Laplace equation of Drop Shape Analysis software (KRUSS). The time step is 200 s between the lines $h = 2.24$, 1.54 and 0.74 mm, and 100 s between the lines $h = 0.74$ and 0.3 mm.

As a first step of analysis we consider the simple heat conduction equation inside the water drop:

$$\Delta T = 0 \quad (3)$$

with a boundary conditions on wall–liquid interface $z = 0$:

$$T = T_w(r) \quad (4)$$

and on liquid–gas interface $z = S(r)$:

$$-\kappa_l \frac{\partial T}{\partial n} = LJ + \alpha(T - T_g) \quad (5)$$

where $T_w(r)$ is a function of wall temperature right under the drop. It can be calculated or measured. κ_l is the thermal conductivity coefficient of liquid, n is a outward vector normal to droplet surface which depends on droplet shape geometry, α is the heat transfer coefficient on the gas–liquid interface, L is the latent heat of vaporization per unit mass, J is the local evaporative mass flux from the droplet. This energy balance condition Eq. (5) allows us to investigate the temperature difference $T(S) - T_g$ influence on heat transfer.

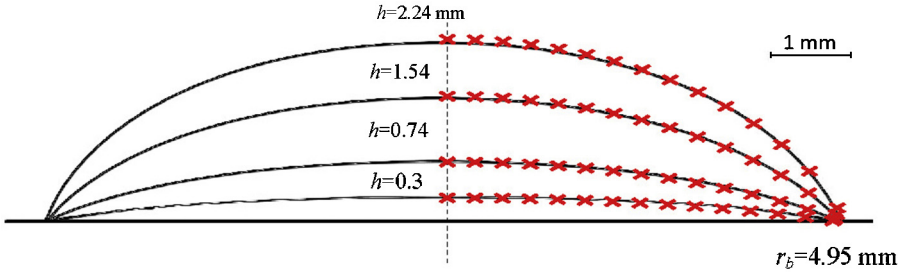

Fig. 3. Evolution of the drop profile for anodized aluminum. Solid lines - experimental data and tics - ellipsoidal shape.

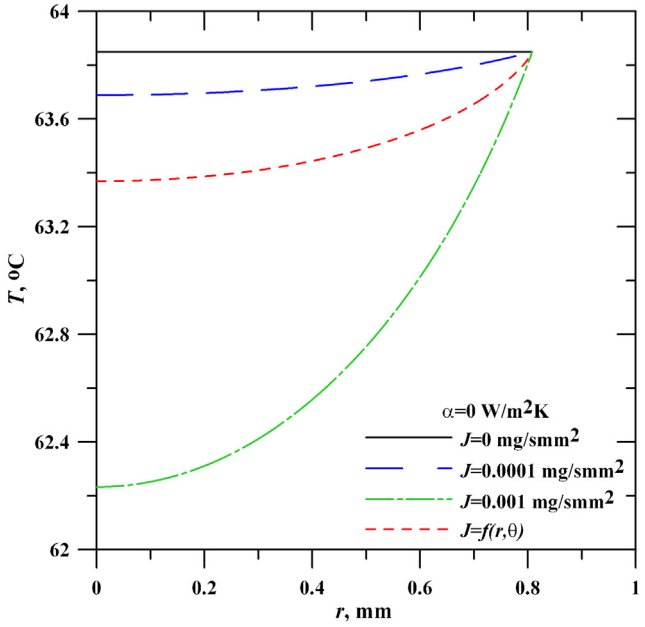

Fig. 4. Temperature distribution on drop surface for different mass flux at $\alpha = 0$. Spin Teflon substrate, droplet volume $V = 0.45$ μl, contact angle $\theta = 55^\circ$, temperature of the solid substrate is constant $T_w = 64\,^\circ$C, temperature of the atmosphere $T_g = 22\,^\circ$C.

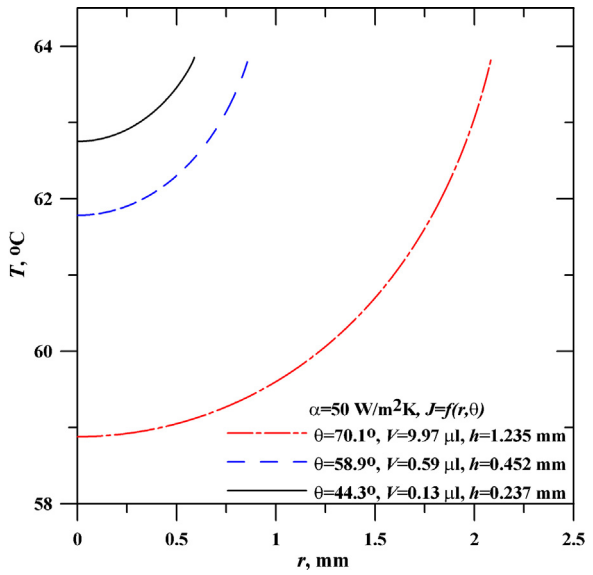

Fig. 5. Effect of droplet volume and contact angle on temperature difference on drop surface. The values of volumes, contact angles are taken from the experiments for different time. Spin Teflon substrate, temperature of the solid substrate is constant $T_w = 64\,^\circ$C, temperature of the atmosphere $T_g = 22\,^\circ$C.

For the case $h/r_b \ll 1$ realizing for the relatively small contact angle the simple approximate solution of Eqs. (3)–(5) exists giving temperature distribution on the droplet surface:

$$T(S) = \frac{\kappa_l T_w + S(r)\left(\alpha T_g - LJ\right)}{\alpha S(r) + \kappa_l} \tag{6}$$

The droplet surface temperature profiles at different mass flux are plotted in Fig. 4 when there is no heat exchange with ambient gas. Four cases are presented: three of them is the temperature distribution on droplet surface when there is a constant mass flux along the droplet surface $J = 0$, 0.0001, 0.001 mg/s mm^2, and the fourth case is the situation when the mass flux $J(r, \theta) = f(r, \theta)$ is a nonuniform function given by Eq. (7) that was proposed in [5] for $0 < \theta < \pi/2$.

$$f(r,\theta) = J_0(\theta)\left(1 - \left(\frac{r}{r_b}\right)^2\right)^{-\lambda(\theta)} \tag{7}$$

$$J_0(\theta) = \frac{Dc_v(1-H)}{r_b}\left(0.27\theta^2 + 1.30\right)\left(0.6381 - 0.2239\left(\theta - \frac{\pi}{4}\right)^2\right)$$

where $\lambda(\theta) = 1/2 - \theta/\pi$, H is the relative humidity of the ambient gas and c_v is the vapor concentration on liquid–gas interface (the saturation value).

It should be noted that $J = 0.001$ mg/s mm^2 is a minimum specific evaporation rate in experiments for this type of surface (see Fig. 13 for details). The temperature field in the droplet changes significantly with evaporation intensity (Fig. 4). However, the difference between the maximum and the minimum temperature on the liquid–gas interface is decreasing with decrease of the droplet volume and contact angle for the same solid temperature T_w and the same ambient gas temperature T_g (Fig. 5).

The heat transport to the gas phase can be of a great importance for cooling of droplet and hence to temperature distribution. Fig. 6 illustrates the droplet surface temperature profiles at different heat transfer coefficients when there is no evaporation. It is shown that the heat exchange with ambient atmosphere has a valuable contribution to the droplet temperature field. Fig. 7 shows the temperature profile on droplet surface when diffusive evaporation and heat exchange with gas phase are both included. The lines are plotted for different heat transfer coefficients. Temperature of the gas–liquid interface has a minimum on the top of the droplet and is increasing with the radius increase. There is a strong increase of temperature close to periphery of the droplet near contact line and the increasing of temperature difference between maximal and minimal surface temperature values. However, for small droplets the value of the minimal droplet surface temperature is close to temperature near the contact line and the average surface temperature is higher than that for the large drops (Fig. 5). This is due to

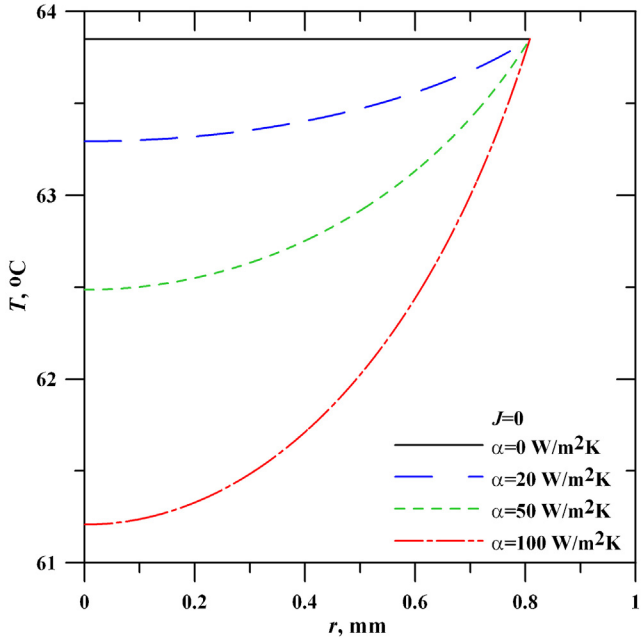

Fig. 6. Temperature distribution on drop surface for different heat transfer coefficient at $J = 0$. Spin Teflon substrate, droplet volume $V = 0.45$ μl, contact angle $\theta = 55^\circ$, temperature of the solid substrate is constant $T_w = 64\,^\circ$C, temperature of the atmosphere $T_g = 22\,^\circ$C.

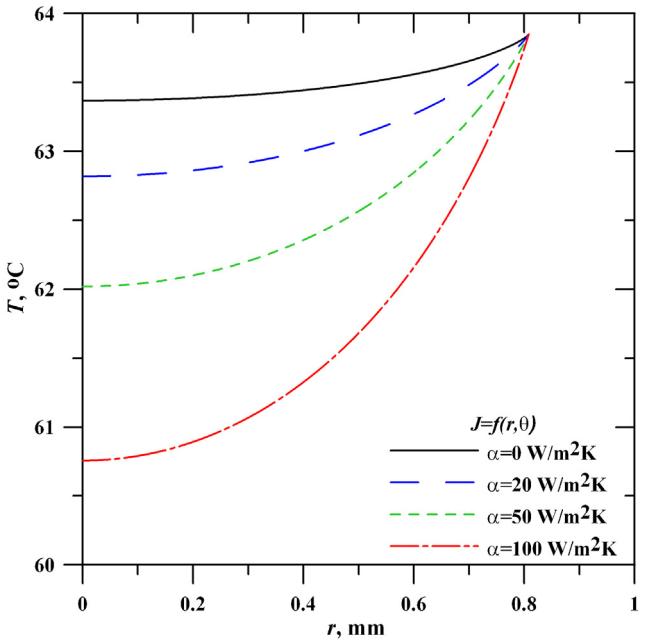

Fig. 7. Temperature distribution on drop surface for different heat transfer coefficient at $J=f(r, \theta)$. Spin Teflon substrate, droplet volume $V=0.45$ μl, contact angle $\theta=55^\circ$, temperature of the solid substrate is constant $T_w = 64^\circ$C, temperature of the atmosphere $T_g=22^\circ$C.

the low amount of liquid that is heated up by the substrate and due to the low thermal resistance of the small size drop. The coupled heat and mass transport to the ambient gas is important for the droplet temperature field. For sufficiently high heat transfer coefficient on the drop surface, $\alpha = 100\,W/m^2K$, the calculation predicts the temperature difference along the drop surface to be 3 °C for the condition of the constant temperature of the solid substrate ($T_w = 64^\circ$C).

4. Droplet evolution during evaporation

4.1. Contact angle and contact radius

We measure the contact angle and contact radius during the droplet evaporation on the substrates with different contact angle hysteresis. We study the effect of contact angle hysteresis on a sessile droplet evolution during evaporation with initial volume V_0. Fig. 8 presents results obtained using the shadow technique. Three modes of droplet evaporation with approximately the same initial volume are recorded: 1 – depinned droplet on Spin Teflon, the contact angle hysteresis $\theta_h = 9.8^\circ$, 2 – partial pinnig on Spray Teflon, the contact angle hysteresis $\theta_h = 29.3^\circ$, and 3 – pinning on anodized aluminum, the contact angle hysteresis $\theta_h = 71.4^\circ$. For large contact angle hysteresis we observe the pinning and for small contact angle hysteresis we observe depinning. As shown in Fig. 9 recorded using shadow technique the contact line remains almost stationary (the contact radius r_b=4.95 mm) and the contact angle decreases to almost zero for evaporating drop on surfaces with a large hysteresis of the contact angle $\theta_h = 71.4^\circ$.

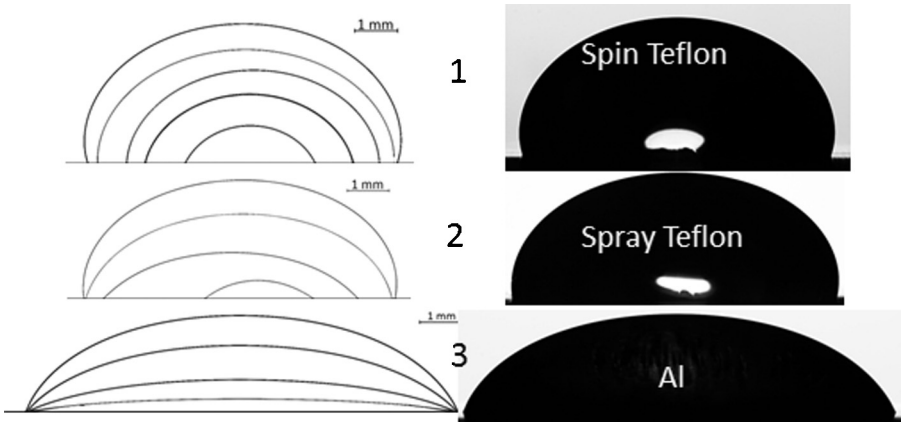

Fig. 8. Drop profile evolution in the process of evaporation for the different substrate: 1 – Spin Teflon ($V_0 = 95.7$ μl, evaporation time $t = 1380$ s), 2 - Spray Teflon ($V_0 = 88.7$ μl, evaporation time $t = 1080$ s), and 3 - anodized aluminum ($V_0 = 104.7$ μl, evaporation time $t = 590$ s).

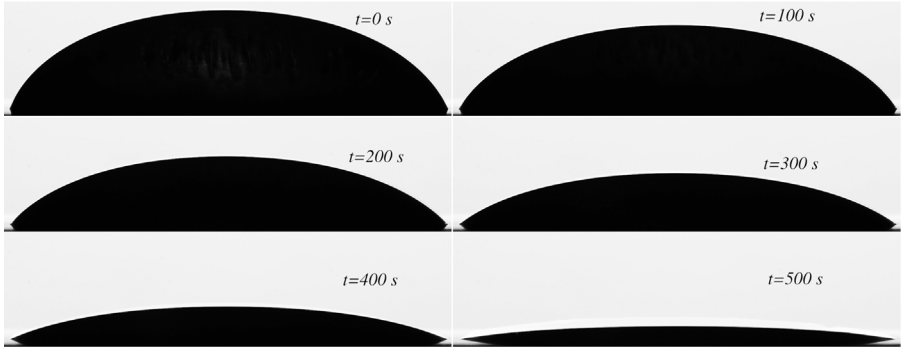

Fig. 9. The evaporating water drop evolution images obtained by shadow technique. The anodized aluminum substrate, initial droplet volume V_0=104.7 μl, temperature of the solid substrate $T_w = 64^\circ$C, temperature of the atmosphere $T_g = 22^\circ$C. Contact radius $r_b = 4.95$ mm. $t = 0$ s: $\theta = 62.4^\circ$, $h = 2.24$ mm; $t = 100$ s: $\theta = 53.2^\circ$, $h = 1.9$ mm; $t = 200$ s: $\theta = 43.1^\circ$, $h = 1.54$ mm; $t = 300$ s: $\theta = 32.6^\circ$, $h = 1.16$ mm; $t = 400$ s: $\theta = 20.7^\circ$, $h = 0.74$ mm; $t = 500$ s: $\theta = 8.4^\circ$, $h = 0.3$ mm.

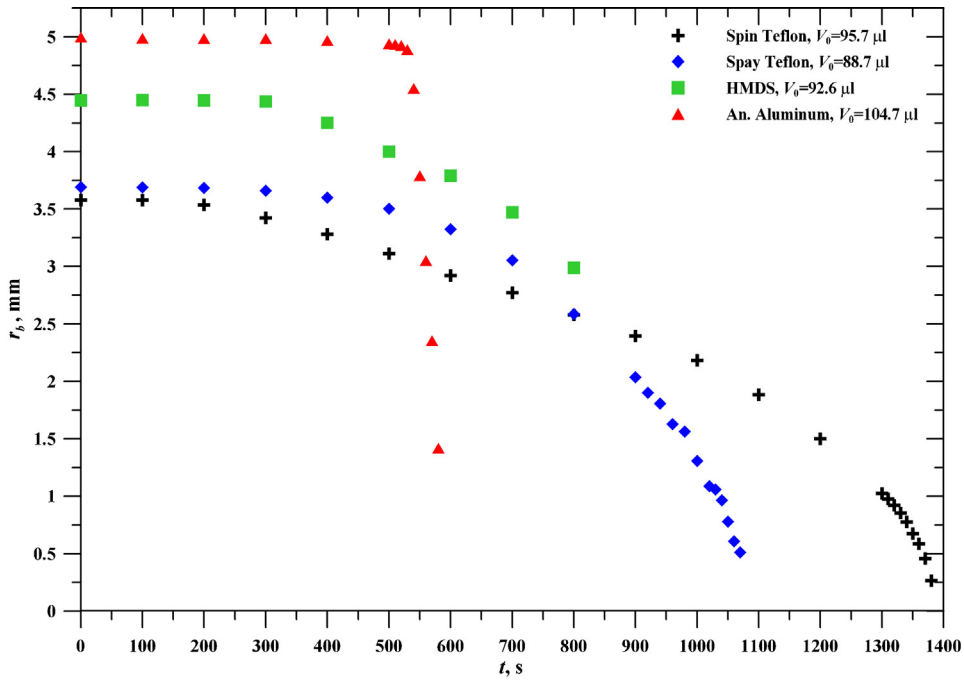

Fig. 10. The contact radius evolution in the process of evaporation for the different substrate. Temperature of the solid substrate $T_w = 64\,^{\circ}C$, temperature of the atmosphere $T_g = 22\,^{\circ}C$. Experimental data.

The behaviors of contact radius and contact angle during evaporation are illustrated in Figs. 10 and 11 respectively. On an anodized aluminum substrate contact line is pinned up to a certain point in time $t \approx 550$ s, so the contact radius r_b remains almost unchanged whereas the contact angle decreases linearly with time. After $t \approx 550$ s the contact radius r_b abruptly decreases. For surfaces with small and moderate contact angle hysteresis the contact radius decreases monotonically (Fig. 10). Experiments on small water droplet on substrate of different wettabilities have been performed by Sobac and Brutin [14]. They provide contact angle evolutions during water droplets evaporation at different substrate temperature for hydrophilic and hydrophobic situation. In the case of a pinned drop (anodized-Al surface in our case) we have qualitative agreement with their results.

We have analyzed different series of experiments for different initial volume of droplet (V_0=95.7 μl, V_0=183.1 μl, V_0=382.0 μl) on

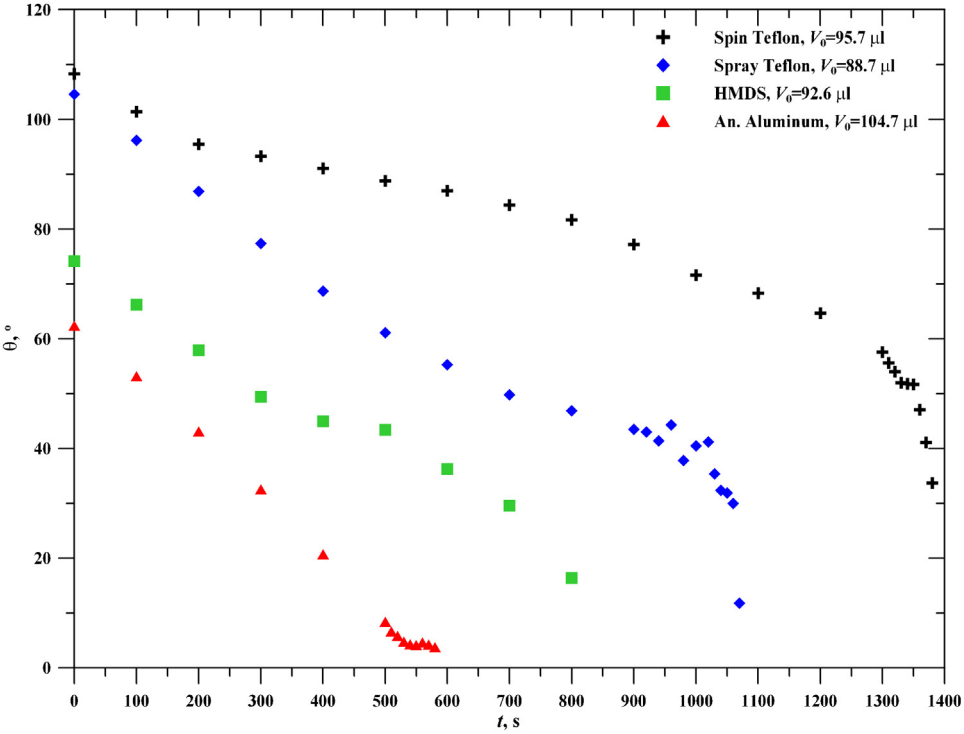

Fig. 11. Contact angle evolution in the process of evaporation for the different substrate. Temperature of the solid substrate $T_w = 64\,^{\circ}C$, temperature of the atmosphere $T_g = 22\,^{\circ}C$. Experimental data.

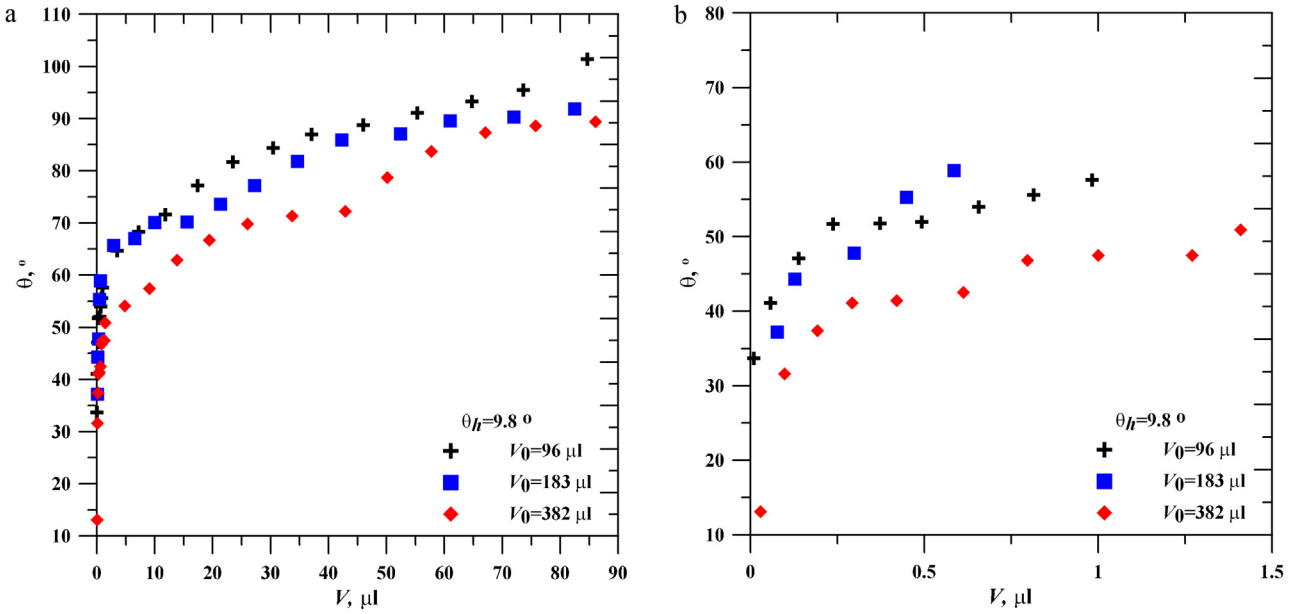

Fig. 12. Contact angle versus volume for different initial volume of water droplet on Spin Teflon. Temperature of the solid substrate $T_w = 64\,^{\circ}$C, temperature of the atmosphere $T_g = 22\,^{\circ}$C. (a) Results in the volume variation from 0 to 90 μl; (b) results in the volume variation from 0 to 1.5 μl. Experimental data.

Spin Teflon substrate which has minimal contact angle hysteresis $\theta_h = 9.8^{\circ}$. The contact angle is monotonically decreasing with decrease of droplet volume during the evaporation process (Fig. 12a and b). From Fig. 12a and b one can see that the difference between the contact angles at the same droplet volume is mostly within the value of the contact angle hysteresis.

4.2. Mass flux and evaporation rate

Determination of the specific evaporation rate and the local evaporative mass flux are extremely important for industrial applications as far as these characteristics evaluate the amount of evaporated liquid per unit area per unit time. The specific evaporation rate *ES* is determined as a ratio of the global evaporation rate $\dot{M}$ to the droplet surface area *A*:

$$ES = \frac{\dot{M}}{A} \tag{8}$$

This is an average characteristic of the evaporative mass flux. For experimental determination of the specific evaporation rate we define it as:

$$ES = \frac{\rho_l \left(V_{r_b+\delta} - V_{r_b-\delta}\right)}{\Delta t \cdot A_{r_b}} \tag{9}$$

where $A_{r_b} = (A_{r_b+\delta} + A_{r_b-\delta})/2$ is the average value of the droplet surface area; $V_{r_b+\delta}$, $A_{r_b+\delta}$ are the volume and surface area of the droplet at the time *t*; $V_{r_b-\delta}$, $A_{r_b-\delta}$ are the volume and surface area of the droplet at the time $t + \Delta t$. Note that volume and surface area are decreasing with time. Fig. 13 demonstrates the specific evaporation rate *ES* versus time. It is found that at the final stage of the drop life specific evaporation rate abruptly increases especially for drops with small and moderate contact angle hysteresis.

We analyze the specific evaporation rate function. At the final stage of evaporation the droplet shape has a spherical cap and the

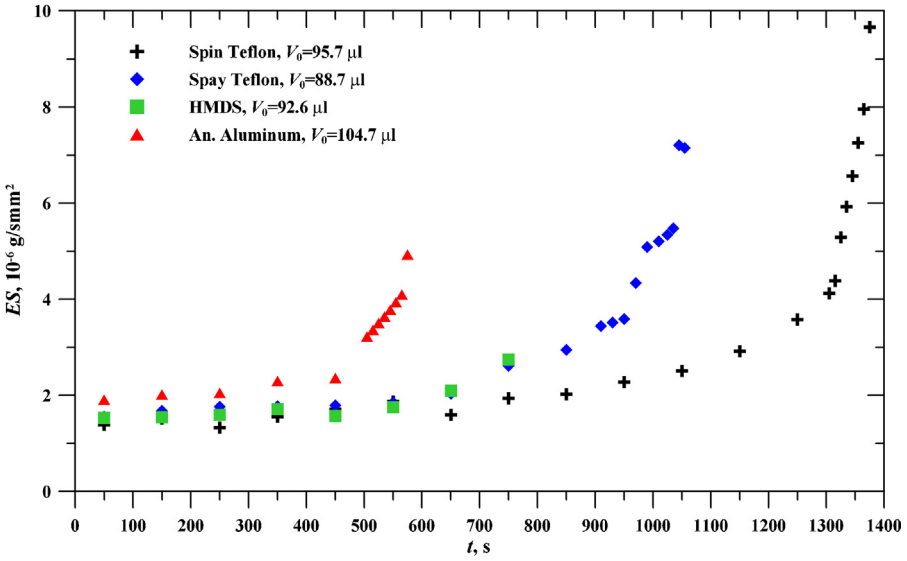

Fig. 13. Specific evaporation rate for different substrates, temperature of the solid substrate $T_w = 64\,^{\circ}$C, temperature of the atmosphere $T_g = 22\,^{\circ}$C. Experimental data.

volume and area can be expressed as a functions of contact radius and the contact angle:

$$V(r_b,\theta)=\frac{\pi r_b^3}{3}\frac{\left(1-\cos\theta\right)^2\left(2+\cos\theta\right)}{\sin^3\theta} \tag{10}$$

$$A(r_b,\theta)=\frac{2\pi r_b^2}{1+\cos\theta} \tag{11}$$

For depinned droplet the volume difference can be approximated as:

$$V_{r_b+\delta}-V_{r_b-\delta}\simeq\frac{\pi}{3}\frac{\left(6r_b^2\delta_r+2\delta_r^3\right)\left(1-\cos\theta\right)^2\left(2+\cos\theta\right)}{\sin^3\theta}$$

where δ_r is the radius variation per time Δt. Then specific evaporation rate is written:

$$ES\simeq\frac{\rho_l\delta_r}{\Delta t}\left(1+\frac{1}{3}\left(\frac{\delta_r}{r_b}\right)^2\right)\frac{\left(1-\cos\theta\right)\left(2+\cos\theta\right)}{\sin\theta}$$

For $\theta\neq 0$ the trigonometric function $\left|\left(1-\cos\theta\right)\left(2+\cos\theta\right)/(\sin\theta)\right|<K$ is a bounded function, where K is the constant. So, the specific evaporation rate:

$$ES\simeq K\frac{\rho_l\delta_r}{\Delta t}\left(1+\frac{1}{3}\left(\frac{\delta_r}{r_b}\right)^2\right) \tag{12}$$

The obtained formula Eq. (12) contains the parameter δ_r which can depend on experimental data and on physical processes such as heat transfer and diffusion. The relation $\delta_r/\Delta t$ can be interpreted as the contact line speed.

In order to describe the evaporation process we consider quasi-steady heat and mass transfer problem. The heat conduction equation inside the water drop:

$$\Delta T=0 \tag{13}$$

and the diffusion equation in gas phase:

$$\Delta C=0 \tag{14}$$

with a boundary conditions on wall-liquid interface $z=0$:

$$T=T_w(r) \tag{15}$$

and on liquid–gas interface $z=S(r)$:

$$-\kappa_l\frac{\partial T}{\partial n}=LJ+\alpha(T-T_g) \tag{16}$$

$$C(T)=C_0+C_1(T-T_g) \tag{17}$$

For simplicity we use a linear approximation of the concentration on the liquid–gas interface on the interfacial temperature. The coefficient C_1 is found from saturated vapor partial pressure tabulations [15–17]:

$$C_1=\frac{(p_1M_v)/(RT_1)-C_0}{T_1-T_g} \tag{18}$$

Here p_1 is a vapor partial pressure at T_1, M_v is a vapor molar mass, R is universal gas constant. $C_0=C_g/H$ where H is the humidity of the air. The temperature T_1 is taken to be equal to the solid substrate temperature T_w. Note that the interfacial concentration $C(T)$ can be approximated polynomially [7] as well as by Wagner equation [18,19]. For our calculations the coefficient C_1 is equal to 4.55×10^{-4} kg/m^{3}K.

The vapor concentration C far away from the liquid droplet $z=\infty$:

$$C(\infty)=C_g \tag{19}$$

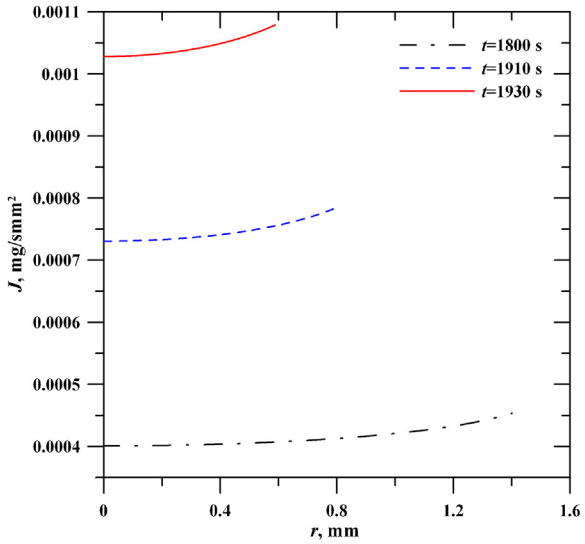

Fig. 14. Local mass flux on droplet surface for different time on Spin Teflon.

Once C is known the local evaporative mass flux from the droplet is given by:

$$J=-D\nabla C\cdot n \tag{20}$$

where D is the coefficient of diffusion of vapor in the atmosphere. For H_2O–air system we use the expression [15]:

$$D(T)=2.05\times10^{-5}\cdot(T/273)^{2.072}\text{m}^2/\text{s} \tag{21}$$

For the calculation of the local mass flux J we organize the iterative procedure. For the first step of calculation the evaporative mass is assumed to be very small 10^{-7} g/s mm^2 (in Eq. (16)) which is an order of magnitude less than the minimum value of the specific evaporation rate at the beginning of the droplet evaporation. Then the second step, we calculate the temperature profile on the droplet surface $T(S)$ which is found out of Eqs. (13), (15), (16). The heat transfer coefficient is $\alpha=50$ W/m^{2}K for our calculations. Knowing the temperature profile on the droplet surface we find the local evaporation mass flux J and the global evaporation rate $\dot{M}$. Then we return to the second step. If the concentration gradient is assumed to be radially outward and two radii of curvature are equal (sherical cap geometry) the local evaporation mass flux is written as:

$$J=D(T)\frac{(C(T)-C_g)}{r_b} \tag{22}$$

Fig. 14 demonstrates the calculated local evaporation mass flux J of depinned water droplet on Spin Teflon for different time $t=1800$ s ($\theta=65.7^\circ$, $r_b=1.4$ mm); $t=1910$ s ($\theta=55.3^\circ$, $r_b=0.8$ mm); $t=1930$ s ($\theta=44.3^\circ$, $r_b=0.6$ mm). The temperature profile on the droplet surface increases close periphery of the drop near the contact line (see Section 3). The temperature field on the drop surface determines the distribution of the vapor concentration (Eq. (17)) and the evaporative mass flux. And the temperature increase along the droplet surface leads to the increase of the evaporative mass flux close to the contact line. Fig. 15 illustrates the mass flux profile J plotted using Eq. (7) (Hu and Larson [5]) with $c_vH=C_g$, $c_v=C(T)$ for the same regimes as for Fig. 14. It should be noted that the mass flux profiles J in Figs. 14 and 15 are very different. This is due to fitting function in Eq. (7) which is not included to our model. Fig. 16 demonstrates our calculations of the local mass flux J for pinned water droplet on anodized aluminum with contact radius $r_b=4.95$ mm and ellipsoidal cap geometry for different time $t=400$ s ($\theta=20.7^\circ$, $h=0.74$ mm); $t=510$ s ($\theta=6.7^\circ$, $h=0.23$ mm); $t=530$ s ($\theta=4.7^\circ$, $h=0.16$ mm). Also, the temperature increase along

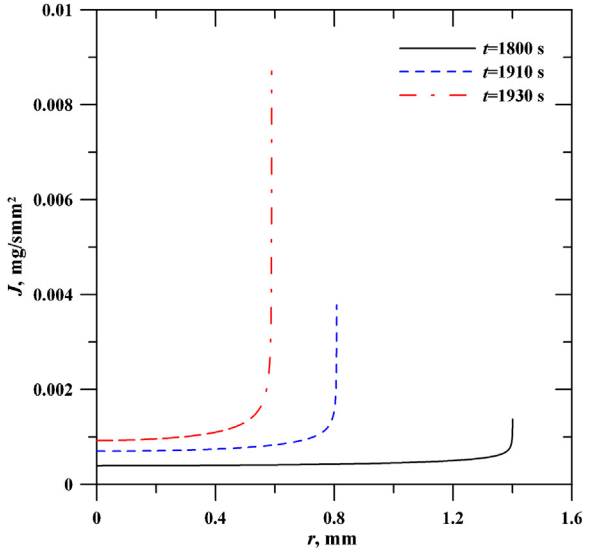

Fig. 15. Local mass flux on droplet surface for different time on Spin Teflon. The temperature dependence of vapor concentration and modified formula Eq. (7) by Hu and Larson [5].

the droplet surface leads to the increase of the evaporative mass flux close to the contact line. And with decrease of droplet height the evaporation intensity increases. One can see more intensive evaporation near the contact line of the droplet with small contact angle.

The specific evaporation rate ES for spherical cap is as follows:

$$ES = \frac{\dot{M}}{A} = \frac{\iint_{\tilde{A}} D(T)(C(T) - C_g)/r_b}{A} \quad (23)$$

where $\tilde{A}$ is a droplet surface, A is a droplet surface area.

The evaporation rate is proportional to the drop perimeter (to the contact radius r_b) while the drop area A is proportional to the

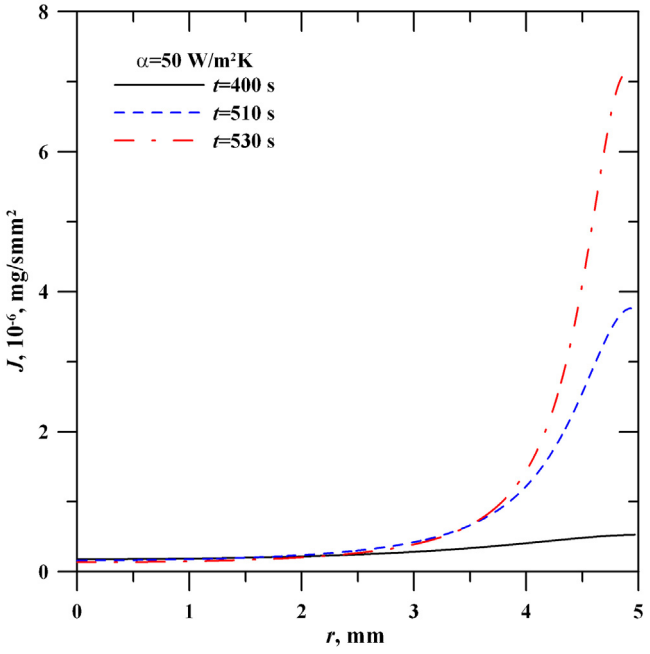

Fig. 16. Local mass flux on the droplet surface for different time on anodized aluminum.

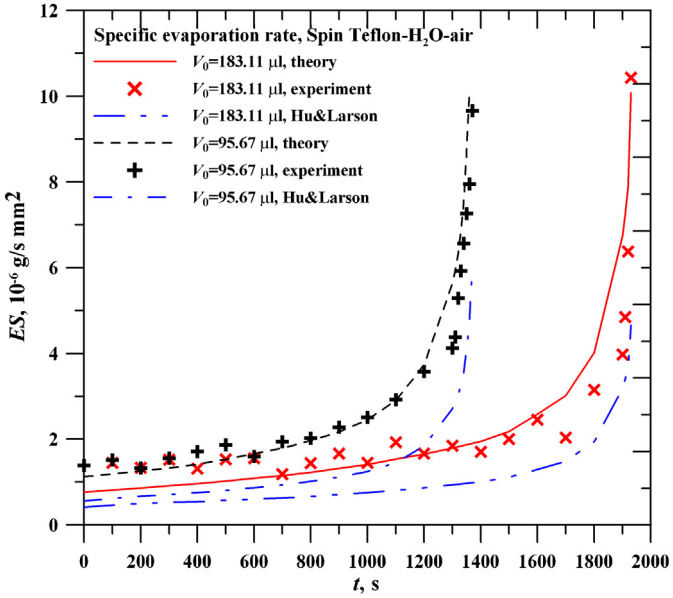

Fig. 17. Specific evaporation rate: experiment and theory. Temperature of the solid substrate $T_w = 64\,^{\circ}$C, temperature of the atmosphere $T_g = 22\,^{\circ}$C.

drop contact radius squared (r_b^2, Eq. (11)). Thus, the specific evaporation rate (evaporation rate per drop area) is a function of $1/r_b$ and diverges at the end of the evaporation when the drop contact radius tends to zero. Present simple model of the drop evaporation allows to estimate the specific evaporation rate. The calculated specific evaporation rate qualitatively and quantitatively agree with experimental data (Fig. 17). The blue lines in Fig. 17 are the specific evaporation rate calculated using the pure diffusive model described in [5] for the constant c_v. The lines are in qualitative agreement.

5. Conclusion

An experimental and theoretical study of the evaporation of a sessile water drop to open atmosphere when the temperature difference between the solid substrate and the atmosphere is about 40 °C has been performed for substrates with different wettability. We investigate all three modes of droplet evaporation: pinning, partial pinning and depinning.

One of the main results of the work is that at the final stage of the drop life the specific evaporation rate abruptly increases especially for drops with small and moderate contact angle hysteresis. The coupled heat and mass transfer model is considered where the temperature field on the drop surface determines the distribution of vapor concentration on liquid–gas interface. The heat exchange of liquid drop with gas phase strongly affects the temperature distribution on the droplet surface. There is a noticeable increase of the temperature close to periphery of the droplet near the contact line. And this leads to the increase of the evaporative mass flux near the contact line. The calculated evaporation rate is proportional to the contact radius r_b while the drop area is proportional to the drop contact radius squared r_b^2. Thus, the specific evaporation rate (evaporation rate per drop area) is a function of $1/r_b$ and diverges at the end of the evaporation when the drop contact radius tends to zero. The calculated specific evaporation rate is in excellent qualitative and quantitative agreement with experimental data. The specific evaporation rate calculated using the pure diffusive model described by Hu and Larson for the constant c_v is in qualitative agreement.

Acknowledgements

The study was supported by The Ministry of Education and Science of Russian Federation, projects 8511, 8745, 14.516.11.0087; RFBR (12-08-31221-mol_a) and Scholarship of the President of RF (SP-160.2012.1).

References

[1] J.C. Maxwell, Diffusion, Collected scientific Papers, Encyclopedia, Britannica, Cambridge, 1877.
[2] V. Sreznevsky, Zh. Russ. Fiz. Khim. Obshchest. 14 (420) (1882) 483.
[3] R.G. Picknett, R. Bexon, The evaporation of sessile or pendant drops in still air, J. Colloid Interface Sci. 61 (1977) 336–350.
[4] B. Sobac, D. Brutin, Triple-line behavior and wettability controlled by nanocoated substrates: influence on sessile drop evaporation, Langmuir 27 (2011) 14999–15007.
[5] H. Hu, R.G. Larson, Evaporation of a sessile droplet on a substrate, J. Phys. Chem. B 106 (2002) 1334–1344.
[6] H.Y. Erbil, Evaporation of pure liquid sessile and spherical suspended drops: a review, Adv. Colloid Interface Sci. 170 (2012) 67–86.
[7] K. Sefiane, S.K. Wilson, S. David, G.J. Dunn, B.R. Duffy, On the effect of the atmosphere on the evaporation of sessile droplets of water, Phys. Fluids 21 (2009) 062101.
[8] M.A. Saada, S. Chikh, L. Tadrist, Evaporation of a sessile drop with pinned or receding contact line on a substrate with different thermophysical properties, Int. J. Heat Mass Transfer 58 (2013) 197–208.
[9] G.J. Dunn, S.K. Wilson, B.R. Duffy, K. Sefiane, Evaporation of a thin droplet on a thin substrate with a high thermal resistance, Phys. Fluids 21 (2009) 052101.
[10] P.L. Kelly-Zion, C.J. Pursell, S. Vaidya, J. Batra, Evaporation of sessile drops under combined diffusion and natural convection, Colloids Surf. A 381 (2011) 31–36.
[11] F. Carle, B. Sobac, D. Brutin, Experimental evidence of the atmospheric convective transport contribution to sessile droplet evaporation, Appl. Phys. Lett. 102 (2013) 061603.
[12] E.A. Chinnov, O.A. Kabov, I.V. Marchuk, D.V. Zaitsev, Heat transfer and breakdown of subcooled falling water film on a vertical middle size heater, Intern. J. Heat Technol. 20 (2002) 69–78.
[13] H.Y. Erbil, R.A. Meric, Evaporation of sessile drops on polymer surfaces: ellipsoidal cap geometry, J. Phys. Chem. B 101 (1997) 6867–6873.
[14] B. Sobac, D. Brutin, Thermal effects of the substrate on water droplet evaporation, Phys. Rev. E 86 (2012) 021602.
[15] Fizicheskie velichiny. Spravochnik. Energoatomizdat, Moskva, 1991.
[16] E.Ya. Gatapova, O.A. Kabov, Shear-driven flows of locally heated liquid films, Int. J. Heat Mass Transfer 51 (2008) 4797–4810.
[17] E.Ya. Gatapova, O.A. Kabov, V.V. Kuznetsov, J.-C. Legros, Evaporating shear-driven liquid film flow in minichannel with local heat source, J. Eng. Thermophys. 13 (2) (2005) 179–197.
[18] R.C. Reid, J.M. Prausnitz, B.E. Poling, The Properties of Gases and Liquids, McGraw-Hill, New York, 1987.
[19] W. Wagner, A. Pruss, International equations for the saturation properties of ordinary water substance. Revised according to the international temperature scale of 1990, J. Phys. Chem. Ref. Data 22 (3) (1993) 783–787.